



HAL
open science

Acoustics of turbulent eddies impinging on a semi-infinite rigid wedge

Marios I Spiropoulos, Florent Margnat, Vincent Valeau, Peter Jordan

► **To cite this version:**

Marios I Spiropoulos, Florent Margnat, Vincent Valeau, Peter Jordan. Acoustics of turbulent eddies impinging on a semi-infinite rigid wedge. AIAA AVIATION 2023 Forum, Jun 2023, San Diego, United States. pp.AIAA 2023-3509, 10.2514/6.2023-3509 . hal-04443650

HAL Id: hal-04443650

<https://univ-poitiers.hal.science/hal-04443650v1>

Submitted on 7 Feb 2024

HAL is a multi-disciplinary open access archive for the deposit and dissemination of scientific research documents, whether they are published or not. The documents may come from teaching and research institutions in France or abroad, or from public or private research centers.

L'archive ouverte pluridisciplinaire **HAL**, est destinée au dépôt et à la diffusion de documents scientifiques de niveau recherche, publiés ou non, émanant des établissements d'enseignement et de recherche français ou étrangers, des laboratoires publics ou privés.

Acoustics of turbulent eddies impinging on a semi-infinite rigid wedge

Marios I. Spiropoulos*, Florent Margnat[†], Vincent Valeau[‡], and Peter Jordan[§]
Institut PPRIME UPR 3346, CNRS - Université de Poitiers - ISAE ENSMA, Poitiers 86022, France

In the present work the far field sound generated by the interaction of isotropic, homogeneous turbulence with a semi-infinite rigid wedge is studied using the theory of vortex sound. The scattering properties of the wedge are modelled with the asymptotic Green's function for the diffraction around a semi-infinite rigid wedge, under the assumption that the source distance from the wedge is acoustically compact. The source term is modelled as a homogeneous, isotropic turbulent quantity and results are shown for different wedge angles and turbulent length scales. Larger eddies dominate the far field sound radiation in the low frequency regime, while smaller ones contribute for higher frequencies and larger wedge angles. The results show that the larger the wedge angle the less noise is generated. A scaling law is obtained that is in agreement with other studies in literature.

I. Introduction

Airfoil noise has been extensively studied numerically, experimentally and theoretical models based on acoustic analogies have been established [1], [2], [3]. The acoustic analogy was introduced by Lighthill (1952), who showed that the sound induced by a turbulent flow is equivalent to a distribution of quadrupole sources [4]. Assuming that the rigid body is acoustically compact, Curle (1955) showed that the aerodynamic fluctuations on a semi-infinite object correspond to a distribution of dipoles which are the dominant sound sources in the absence of moving surfaces and change of mass flow rate [5]. These dipole sources have an acoustic intensity that scales with the sixth power of the fluid velocity (U^6). Ffowcs Williams and Hall (1970) used Lighthill's acoustic analogy and the half-plane Green's function to argue that turbulent quadrupole sources very close to a semi-infinite half plane with a sharp edge result in an acoustic intensity that scales to the fifth power of the turbulent velocity [6]. Crighton and Leppington (1971) illustrated that the far field acoustic intensity of a turbulent flow interacting with the edge of a semi-infinite wedge scales with a law that depends on the wedge angle, when the sound wavelength is much larger than the principle dimension of the obstacle [7]. Other researchers used a different approach by relating the hydrodynamic pressure spectrum on the airfoil to the acoustic power spectral density [8]. Amiet [9], [10] based on Curle's analogy, derived an analytical model for estimation of the far-field generated noise when a turbulent gust interacts with the trailing edge of an airfoil. Amiet's model was later extended to lower frequencies and non-uniform flows [11], [12], [13]. Trafny et al [14] proposed a semi-analytical model for the prediction of airfoil noise, using Lighthill's acoustic analogy and an approximate Green function for half planes, proposed by Howe (2001) [15].

The theory of vortex sound, introduced by Howe (1975) [16], can be considered a special case of Lighthill's analogy for low Mach number flows [17]. Howe derived a general solution for the aerodynamic sound generated by the flow around a rigid semi-infinite plane using the theory of vortex sound [18] in an attempt to unify different trailing-edge noise theories.

Most of the analytical airfoil-noise models in literature replace the leading and trailing edges with semi-infinite half planes. The shape of the airfoil is supposed to influence only the flow around it, or it is taken into consideration by introducing correcting factors as shown by Gershfeld (2004) [19]. In practice, the bluntness of the leading edge and the sharpness of the trailing edge impose different flow and scattering conditions. In the present work, the aerodynamic noise generated by turbulent, low-Mach-number flows at the airfoil edges is examined. The scattering properties of the airfoil edges are approximated by semi-infinite acoustically rigid wedges with half angle Ω . The distance of the source term to the edges is assumed to be acoustically compact $k_0 r_0 \ll 1$ and the turbulence homogeneous and isotropic. The derivation of this simple model is based on the reasoning of Amiet's work [9] in the sense that the source is modelled

*Graduate Student, marios.spiropoulos@univ-poitiers.fr

[†]Assistant Professor, florent.margnat@univ-poitiers.fr

[‡]Professor, vincent.valeau@univ-poitiers.fr

[§]Research Director, peter.jordan@univ-poitiers.fr

as a statistical quantity. In Section II the mathematical problem is formulated based on the works of Amiet [9] and Howe [20]. Furthermore, the source term of Howe's theory of vortex sound is analysed and written as a function of the turbulent kinetic energy spectrum (Section III). In Section IV the turbulence close to the wedge is assumed to consist of one region with small turbulent eddies very close to the edge (inner region) and an outer region with larger turbulent structures that are convected downstream. For purposes of illustration, the von Karman turbulent spectrum is used and the two different turbulent length scales of the inner and outer region are compared in Section V. Finally, an analytical expression for the far-field power spectral density is obtained and the results are discussed.

II. Problem formulation

Let a body immersed in a turbulent flow convected with a velocity U across the y_1 -axis as shown in Figure 1. The coordinate system of the source and the observer are given by the position vectors in cartesian coordinates $\vec{y} = (y_1, y_2, y_3)$, $\vec{x} = (x_1, x_2, x_3)$ respectively. For future reference, the polar coordinates will be denoted as (r_0, θ_0) for the source and (r, θ) for the observer. In applications of low-Mach-number flows ($M < 0.3$) [21], the theory of vortex sound can be used in the following form [22]

$$p(\vec{x}, t) = -\rho \int_t \int_V s_m \frac{\partial G}{\partial y_m}(\vec{x}; \vec{y}, t - \tau) dy_1 dy_2 dy_3 dt \quad (1)$$

where $p(\vec{x}, t)$ the acoustic pressure measured by an observer in the far-field, $s_m = (\vec{\omega} \times \vec{v})_m$ the source, expressed as the cross product of the vorticity with the velocity field and τ the propagation time of the acoustic waves. The tailored Green's function (G) describes the scattering of the source by the surface of the obstacle immersed in the flow. A summation over $m=1,2,3$ is implied. The source term can be written in frequency space by assuming that

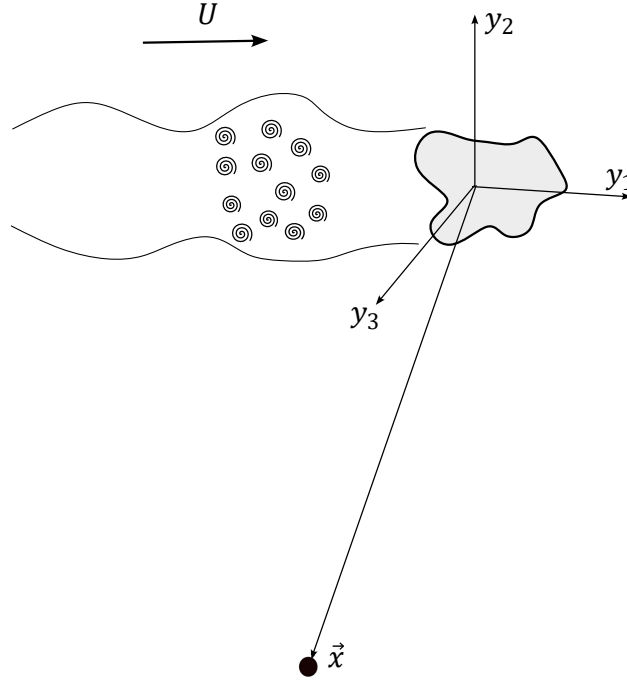


Fig. 1 Turbulent flow impinging on a rigid body. Vectors \vec{y} , \vec{x} correspond to the coordinates of the source and the far-field observer. The turbulent eddies are convected with velocity U across the y_1 -axis.

$$s_m(\vec{y}, t) = S_m(\vec{y}, \omega) e^{-i\omega(t-\tau)}.$$

It yields:

$$P(\vec{x}, \omega) = -\rho \int_V S_m(\vec{y}, \omega) \frac{\partial G}{\partial y_m}(\vec{x}; \vec{y}, \omega) dy_1 dy_2 dy_3 \quad (2)$$

In order to facilitate the analysis the inverse wave-number transform is applied and the source is represented as:

$$S_m(\vec{y}, \omega) = \iint_{-\infty}^{\infty} \hat{S}_m(k_1, k_2) e^{i(k_1 y_1 + k_2 y_2)} dk_1 dk_2, \quad (3)$$

where \hat{S}_m is the source as a function of the wave-numbers k_1, k_2 . Furthermore, we assume that the turbulent fluctuations are convected by a velocity U . Hence we may write:

$$\hat{S}_m(\omega, k_1, k_2, y_3) = \hat{S}_m(\omega, k_2, y_3) \delta(k_1 - \omega/U)$$

where δ is the Dirac δ -function. Equation (2) becomes:

$$P(\vec{x}, \omega) = -\rho \int_{-\infty}^{\infty} dk_2 \iiint_{-\infty}^{\infty} \hat{S}_m(\omega/U, k_2, y_3) \frac{\partial G}{\partial y_m}(\vec{x}; \vec{y}, \omega) e^{i(\frac{\omega}{U} y_1 + k_2 y_2)} dy_1 dy_2 dy_3 \quad (4)$$

It is convenient to model the source term as statistical quantity since it consists of the turbulent velocity and vorticity fluctuations. To calculate the far field acoustic power spectral density the correlation of two points in the turbulent flow $(y_1, y_2, y_3), (y'_1, y'_2, y_3)$ needs to be computed. Following the same steps as in [9]:

$$\begin{aligned} \langle PP^* \rangle(\vec{x}, \omega) &= -\rho^2 \int_{-\infty}^{\infty} dy_3 \iint_{-\infty}^{\infty} \langle \hat{S}_m(\omega/U, k_2, y_3) \hat{S}'_m(\omega/U, k'_2, y_3) \rangle e^{ik_2(y_2 - y'_2)} dk_2 dk'_2 \times \\ &\quad \times \iiint_{-\infty}^{\infty} \frac{\partial G}{\partial y_m} \frac{\partial G^*}{\partial y'_m} e^{i\frac{\omega}{U}(y_1 - y'_1)} dy_1 dy_2 dy'_1 dy'_2, \end{aligned} \quad (5)$$

where the asterisk (*) denotes the complex conjugate. Due to the statistical orthogonality of the wave-vectors [9], it yields

$$\langle \hat{S}_m(\omega/U, k_2, y_3) \hat{S}'_m(\omega/U, k'_2, y_3) \rangle = \phi_{ij}^m(\omega/U, k_2, y_3) \delta(k_2 - k'_2) \quad (6)$$

where $\phi_{ij}^m(\omega/U, k_2, y_3)$ the power spectrum of the source. Supposing that the source is a statistically stationary quantity in space, we calculate the auto-correlation length scale

$$l_{y_3}(\omega) = 2 \frac{\int_0^{L/2} \phi_{ij}^m(\omega/U, k_2, y_3) dy_3}{\phi_{ij}^m(\omega/U, k_2, 0)} \quad (7)$$

where $\phi_{ij}^m(\omega/U, k_2, 0)$ denotes the source power spectrum at the mid-span and L the span.

From Eqs. (5), (6), (7) the far field acoustic power spectral density is written as follows:

$$\langle PP^* \rangle(\vec{x}, \omega) = -l_{y_3}(\omega) \rho^2 \iiint_{-\infty}^{\infty} \left(\int_0^{\infty} \phi_{ij}^m(\omega/U, k_2, 0) e^{ik_2(y_2 - y'_2)} dk_2 \right) \frac{\partial G}{\partial y_m} \frac{\partial G^*}{\partial y'_m} e^{i\frac{\omega}{U}(y_1 - y'_1)} dy_1 dy_2 dy'_1 dy'_2 \quad (8)$$

At this step we assumed that the Green function has no dependence on the span-wise coordinate $G = G(y_1, y_2)$. This hypothesis is based on the fact that we are studying the problem as two-dimensional and will be justified later in sub-section IV.C.

III. Source modelling

As shown in Equation (8), the phenomenon is described by a statistical term (source's turbulent spectrum) and a deterministic one that depends on the scattering properties of the object immersed in the flow (Green's function). The problem will be treated as two dimensional, therefore the source will be modelled at the midspan. Any variation in the

span-wise direction is contained in the span-wise correlation length $l_{y_3}(\omega)$. As a result, the velocity and vorticity fields are given as follows

$$\begin{aligned}\vec{v} &= (U + u_1, u_2, 0) \\ \vec{\omega} &= (0, 0, \Omega_3).\end{aligned}$$

It is noted that in the present section, all quantities are written in the wave-number space, unless stated otherwise. The wavenumber vector is the same as the one introduced in Section II. Expanding the cross product it yields:

$$\vec{\hat{S}}(\vec{k}) = \vec{\omega}(\vec{k}) \times \vec{v}(\vec{k}) = -u_2(\vec{k})\Omega_3(\vec{k})\hat{e}_1 + (U\Omega_3(\vec{k}) + u_1(\vec{k})\Omega_3(\vec{k}))\hat{e}_2 \quad (9)$$

The convection velocity is assumed greater than the fluctuations of the velocity field in the stream-wise direction $U \gg u_1$ and therefore:

$$\hat{S}(\vec{k}) = -u_2(\vec{k})\Omega_3(\vec{k})\hat{e}_1 + U\Omega_3(\vec{k})\hat{e}_2 \quad (10)$$

The solenoidal component of the velocity field is the one that contributes mostly to the acoustic radiation as shown by Goldstein's rapid distortion theory [23]. Howe (1998) calculates the latter as [20] :

$$\vec{u}(\vec{k}) = i\vec{k} \times \vec{\omega}(\vec{k}) / k^2 \quad (11)$$

where $k = \sqrt{(\omega/U)^2 + k_2^2}$, the hydrodynamic wavenumber. Combining Eqs (10), (11) we get

$$\hat{S} = \begin{bmatrix} \Omega_3^2(\omega/U, k_2) \frac{\omega U}{\omega^2 + U^2 k_2^2} \\ U\Omega_3(\omega/U, k_2) \end{bmatrix} \quad (12)$$

and the source power spectrum of Equation (6) becomes:

$$\phi_{ij}(\omega/U, k_2, 0) = U^2 \left[\frac{\langle \Omega_3^2 \Omega_3'^2 \rangle \omega^2 (\omega^2 + U^2 k_2^2)^{-2}}{\langle \Omega_3 \Omega_3' \rangle} \right] \quad (13)$$

Then substituting Equation (13) into Equation (8), the latter takes the following form:

$$\langle PP^{*} \rangle(\vec{x}, \omega) = -\rho^2 l_{y_3}(\omega) \iiint_{-\infty}^{\infty} \left[\int_0^{\infty} \phi_{ij}^m(\omega/U, k_2, 0) e^{i(k_2(y_2 - y_2'))} dk_2 \right] \frac{\partial G}{\partial y_m} \frac{\partial G^*}{\partial y_m'} e^{i(\frac{\omega}{U}(y_1 - y_1'))} dy_1 dy_2 dy_1' dy_2' \quad (14)$$

IV. Turbulent regions close to the edge

Equation (14) describes the acoustic power spectral density generated by the interaction of a turbulent flow close to an obstacle. It can be seen that there exist two sources in the flow that can be considered as two dipoles oriented perpendicularly. The first one, in the transverse direction, depends on the turbulent vorticity spectrum, while the second one depends on the square of the vorticity fluctuations and is oriented in the stream-wise direction. In the present work, we assume that the non-linear source is much weaker and the main contribution to the sound radiation comes from $U^2 \langle \Omega_3 \rangle$. However, these quantities can be obtained by experimental data or numerical simulations, for different kinds of flow conditions around edges i.e. boundary layers, wakes etc. In the present section, results will be shown for two simplified cases: i) small eddies that lie very close to the edges of the airfoils with a turbulent length scale equal to their distance from the edge and ii) larger turbulent eddies that are convected by the wake or boundary layer velocity U . Figure 2 shows a sketch of these turbulent regions close to an edge. From now on we will call the red region of Fig. 2 *inner region* and the one with the larger (black) eddies *outer region*. The boundaries of the inner and outer regions are defined as follows. For sources that exist in the inner region

$$r_0 \in [\epsilon, \xi],$$

where ϵ is chosen to be very close to the edge, and ξ a length scale that is used to define the boundaries of the inner region. $r_0 = \sqrt{y_1^2 + y_2^2}$ corresponds to the radial source distance from the edge of the wedge. For sources in the outer region it holds

$$r_0 \in [\xi, X],$$

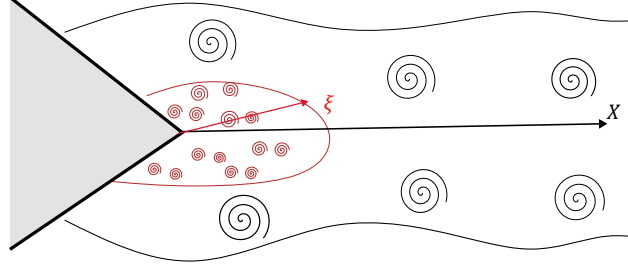


Fig. 2 The wake is split into two regions. One of small size eddies located very close to the edge and an outer region with larger convected eddies.

where X the total extent of the wake. In the present analysis these length scales will be chosen arbitrarily for purposes of illustration of the model, however their values could be inferred by detailed experiments or numerical simulations.

A. Inner region

Inside this region the distance between two correlated turbulent eddies can be considered comparable to the turbulent length scale $l_{in}(r_0)$, which has a dependence on their distance from the edge of the wedge. Hence, we may write

$$\frac{\omega}{U} (y_1 - y'_1) = \frac{\omega l_{in}(r_0)}{U}.$$

The boundary layer or the wake thickness is much smaller than its extent in the stream-wise dimension and therefore the correlation distance in the stream-wise direction is more important than the one in the transverse direction, and we may assume that

$$k_2 (y_2 - y'_2) \ll \frac{\omega l_{in}(r_0)}{U}.$$

As a result the far field power spectral density is obtained by:

$$\langle PP^* \rangle_{in}(\vec{x}, \omega) = -\rho^2 \Phi^m |R_{in_m}|^2 l_{y_3}(\omega)$$

$$R_{in_m} = \iint_{-\infty}^{\infty} e^{i \frac{\omega}{U} l_{in}(r_0)} \frac{\partial G}{\partial y_m} dy_1 dy_2 \quad (15)$$

$$\Phi^m = \int_0^{\infty} \phi_{ij}^m dk_2$$

where the components of ϕ_{ij}^m are given by Eq.(13). Detailed steps of the derivation are shown in Appendix A.

B. Outer region

The outer region is occupied by larger eddies, convected far from the edge. Therefore, we assume that the convection effect alters the stream-wise position of the source (y_1). The thickness of the boundary layer (or the wake) (δ) is much smaller than the extend of the boundary layer (or wake) in the stream-wise direction and we introduce a length scale that describes the eddies of the outer region

$$y_2 - y'_2 = \Delta y \approx l_{out} \quad (16)$$

where $l_{out} < \delta$. Then, Eq.(14) yields

$$\langle PP^* \rangle_{out}(\vec{x}, \omega) = -\rho^2 \Xi^m |R_{out_m}|^2 l_{y_3}(\omega)$$

$$R_{out_m} = \iint_{-\infty}^{\infty} \frac{\partial G}{\partial y_m} e^{i\omega y_1/U} dy_1 dy_2 \quad (17)$$

$$\Xi^m = \int_0^{\infty} e^{ik_2 l_{out}} \phi_{ij}^m dk_2$$

The responses R_{in}, R_{out} of Eqs. (15), (17) can be calculated analytically for simple shapes or numerically for more complicated ones. Keeping only the linear component of the source term the far field power spectral density can be given by the following expression:

$$\langle PP^* \rangle(\vec{x}, \omega) = -\rho^2 \left[\frac{\Xi^{(2)} |R_{out_2}|^2}{\Phi^{(2)} |R_{in_2}|^2} \right] l_{y_3}(\omega) \quad (18)$$

$$\begin{bmatrix} R_{out_2} \\ R_{in_2} \end{bmatrix} = \iint_{-\infty}^{\infty} \frac{\partial G}{\partial y_2} \begin{bmatrix} e^{i\omega y_1/U} \\ e^{i\omega l_{in}(r_0)/U} \end{bmatrix} dy_1 dy_2$$

It has thus been established, that the acoustic field is the product of a turbulent spectrum, a response function and a span-wise correlation length. This lies in agreement with Amiet's model and its extentions [9], [11], [12]. Amiet assumed a pressure jump across the airfoil, which depends on a dipole force exerted on the fluid and an unsteady upwash velocity which is modelled as the statistical quantity. So far, the main difference between the latter and the proposed approach is that the source term is modelled with the theory of vortex sound [20]. Furthermore, the turbulence around the edge is described by two regions, that each one corresponds to smaller (inner) and larger (outer) structures and it will be shown that each region has a different contribution to the acoustic field.

C. Application to Edge Noise

By choosing appropriately the flow conditions and the Green function that describe the scattering of sound by an obstacle immersed in the flow, Eqs. (18) can estimate the far field generated sound by turbulent flows impinging on arbitrary shapes. Depending on the choise of the Green's function, the integration can be performed in other coordinate systems thus for

$$\vec{y} = \vec{y}(p, q)$$

the following formulation can be used

$$\begin{bmatrix} R_{out_2} \\ R_{in_2} \end{bmatrix} = \int_{p_1}^{p_2} \int_{q_1}^{q_2} |J| \left(\frac{\partial G}{\partial p} \frac{\partial p}{\partial y_2} + \frac{\partial G}{\partial q} \frac{\partial q}{\partial y_2} \right) \begin{bmatrix} e^{i\omega y_1(p,q)/U} \\ e^{i\omega l_{in}(r_0)/U} \end{bmatrix} dp dq \quad (19)$$

where $|J|$ the Jacobian determinant. Thus, it is noted that Eq. (19) can be applied generally to any type of scattering surface, as long as its Green's function is known.

In most analytical or semi-analytical models, the effect of thickness at the leading or trailing edge is considered to influence only the flow field and its diffraction properties are not taken into account [3], [10], [11], [14], [15], [24], [25]. In the experimental study of Celik et al [26] it was shown that the greater the angle of a beveled trailing edge the less sound is generated in the far field. In order to investigate the effect of the angle of the trailing or leading edge, the Green function for the wedge scattering will be used in Eq. (19). The airfoil edges will be considered to be far enough apart such that each contribution to the far field noise can be considered separately. For an observer in the far field the 3D Green function can be approximated by an equivalent 2D Green function via the method of stationary phase [27]. The equivalent 2D Green function for the sound scattering around a rigid semi-infinite wedge and an observer in the far field

is given by the following expression in polar coordinates [20].

$$G(r, \theta; r_0, \theta_0, \omega) = -\frac{1}{2r} \sum_{n=0}^{\infty} \sigma_n J_{n/\gamma}(kr_0 \sin \psi) \cos\left(n \frac{\theta - \pi}{\gamma}\right) \cos\left(n \frac{\theta_0 - \pi}{\gamma}\right) e^{ikr - in\pi/(2\gamma)} \quad (20)$$

where ψ denotes the angle between the observer and the edge of the wedge, $r = |\vec{x} - y_3 \vec{e}_3|$, $\sigma_0 = 1/(\gamma\pi)$, $\sigma_n = 2\sigma_0$, $n \geq 1$ and $\gamma = 2(\pi - \Omega)/\pi$ will be called the wedge parameter. Turbulent eddies that lie closer to the edge tend to contribute more to the far field noise. Therefore, we will work under the assumption that the distance of the source to the edge is small enough compared to the wave-length so that it can be considered acoustically compact $k_0 r_0 \ll 1$. The asymptotic form of the Bessel function for small arguments can be applied [28] and Eq.(20) becomes ([29], [20], [27]):

$$G(r, \theta; r_0, \theta_0, \omega) = -\frac{e^{i(k|\vec{r}| - \pi/(2\gamma))} (k \sin \psi/2)^{1/\gamma} r_0^{1/\gamma}}{\gamma\pi|\vec{r}|\Gamma(1/\gamma + 1)} \cos\left(\frac{\theta - \pi}{\gamma}\right) \cos\left(\frac{\theta_0 - \pi}{\gamma}\right) \quad (21)$$

where $\Gamma(\dots)$ the gamma-function. Taking the derivatives of Equation (21) yields

$$\frac{\partial G}{\partial r_0} = -\frac{e^{i(k|\vec{r}| - \pi/(2\gamma))} (k \sin \psi/2)^{1/\gamma} r_0^{1/\gamma - 1}}{\gamma^2 \pi |\vec{r}| \Gamma(1/\gamma + 1)} \cos\left(\frac{\theta - \pi}{\gamma}\right) \cos\left(\frac{\theta_0 - \pi}{\gamma}\right) \quad (22)$$

$$\frac{\partial G}{\partial \theta_0} = \frac{e^{i(k|\vec{r}| - \pi/(2\gamma))} (k \sin \psi/2)^{1/\gamma} r_0^{1/\gamma}}{\gamma\pi|\vec{r}|\Gamma(1/\gamma + 1)} \cos\left(\frac{\theta - \pi}{\gamma}\right) \sin\left(\frac{\theta_0 - \pi}{\gamma}\right)$$

Changing into polar coordinates Eq.(19) reduces to

$$\begin{bmatrix} R_{out_2} \\ R_{in_2} \end{bmatrix} = \int_{\epsilon}^{r_{0,max}} \int_{\theta_{0,1}}^{\theta_{0,2}} \left(\frac{\partial G}{\partial r_0} r_0 \sin(\theta_0) - \frac{\partial G}{\partial \theta_0} \cos(\theta_0) \right) \begin{bmatrix} e^{i\omega r_0 \cos(\theta_0)/U} \\ e^{i\omega l_{in}(r_0)/U} \end{bmatrix} dr_0 d\theta_0 \quad (23)$$

Where $r_{0,max}$, $\theta_{0,1}$, $\theta_{0,2}$, correspond to the volume in which the source region is integrated and $\epsilon \rightarrow 0$ is the closest distance of the source to the edge. For brevity we refer to R_{out_2} , R_{in_2} as R_{out} , R_{in} .

D. Wake at a trailing edge

An illustration will be shown for the trailing edge of an airfoil, however similar arguments can be made for the leading edge as well. The wake is extended to a distance X in the streamwise direction. The thickness of the wake δ is considered to be small enough such that the maximum source distance depends mainly on the position of the source in the stream-wise direction.

$$r_{0,max} = \sqrt{\delta^2/4 + X^2} \approx X$$

Figure 3 shows the geometry of the problem in more detail.

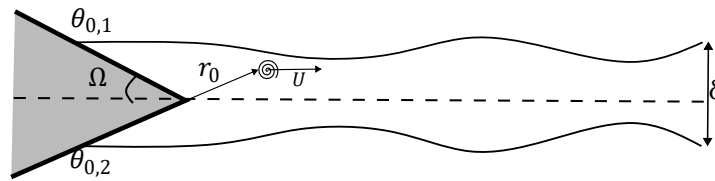


Fig. 3 The wake close to the trailing edge of the airfoil. The integration region is considered to be the wake extended in the stream-wise axis, with thickness δ . The turbulent fluctuations of vorticity are convected with the wake velocity U .

The response function of Eq. (23) reads:

$$\begin{aligned} \begin{bmatrix} R_{out} \\ R_{in} \end{bmatrix} &= -\frac{e^{i(k|\bar{r}|-\pi/(2\gamma))} (k \sin \psi/2)^{1/\gamma}}{\gamma^2 \pi |\bar{r}| \Gamma(1/\gamma + 1)} \cos\left(\frac{\theta - \pi}{\gamma}\right) \\ &\int_{\epsilon}^X r_0^{1/\gamma} \int_{\theta_{0,1}}^{\theta_{0,2}} \left(\cos\left(\frac{\theta_0 - \pi}{\gamma}\right) \sin(\theta_0) - \sin\left(\frac{\theta_0 - \pi}{\gamma}\right) \cos(\theta_0) \right) \times \\ &\times \begin{bmatrix} e^{i\omega r_0 \cos(\theta_0)/U} \\ e^{i\omega l_{in}/U} \end{bmatrix} dr_0 d\theta_0 \end{aligned} \quad (24)$$

Equation (24) can be simplified further, by using the following trigonometric identity

$$\cos(x) \sin(y) - \sin(x) \cos(y) = -\sin(x - y)$$

$$\begin{aligned} \begin{bmatrix} R_{out} \\ R_{in} \end{bmatrix} &= -\frac{e^{i(k_0|\bar{r}|-\pi/(2\gamma))} (k_0 \sin \psi/2)^{1/\gamma}}{\gamma^2 \pi |\bar{r}| \Gamma(1/\gamma + 1)} \cos\left(\frac{\theta - \pi}{\gamma}\right) \times \\ &\times \int_{\epsilon}^X r_0^{1/\gamma} \int_{\theta_{0,1}}^{\theta_{0,2}} \sin\left(\frac{\pi + (\gamma - 1)\theta_0}{\gamma}\right) \begin{bmatrix} e^{i\omega r_0 \cos(\theta_0)/U} \\ e^{i\omega l_{in}/U} \end{bmatrix} dr_0 d\theta_0 \end{aligned} \quad (25)$$

1. Application to inner region

The inner region consists of smaller eddies that lie very close to the edge.

$$\begin{aligned} R_{in} &= -M^{1/\gamma} \left(\frac{U}{\omega}\right) \frac{e^{i(k_0|\bar{r}|-\pi/(2\gamma))} (k_0 \sin \psi/2)^{1/\gamma}}{\gamma^2 \pi |\bar{r}| \Gamma(1/\gamma + 1)} \cos\left(\frac{\theta - \pi}{\gamma}\right) \times \\ &\times \int_{\frac{\omega\epsilon}{U}}^{\frac{\omega\xi}{U}} \int_{\Omega}^{\pi} e^{i\omega l_{in}(r_0)/U} \left(\frac{\omega r_0}{U}\right)^{1/\gamma} \sin\left(\frac{\pi + (\gamma - 1)\theta_0}{\gamma}\right) d\left(\frac{\omega r_0}{U}\right) d\theta_0 \end{aligned} \quad (26)$$

where $M = U/c_0$ the Mach number. Very close to the edge we assume that the length scale is equivalent to the edge distance

$$l_{in}(r_0) = r_0.$$

Then it follows

$$R_{in} = -\frac{2M^{1/\gamma} \left(\frac{U}{\omega}\right) \cos\left(\frac{\theta - \pi}{\gamma}\right) e^{i(k_0|\bar{r}|-\pi/(2\gamma))} (\sin \psi/2)^{1/\gamma}}{\gamma^2 \pi |\bar{r}| \Gamma(1/\gamma + 1)} \left(\frac{2(\pi - \Omega)(\sin(\Omega) - 1)}{\pi - 2\Omega}\right) \int_{\frac{\omega\epsilon}{U}}^{\frac{\omega\xi}{U}} e^{i\alpha} \alpha^{1/\gamma} d\alpha, \quad (27)$$

2. Application to outer region

In the outer region, the turbulent eddies generated at the trailing edge are convected downstream. They contribute to the far field sound as in Eq. (17). Equation (25) is modified and the integration is performed in $r_0 \in [\xi, X]$ and $\theta_0 \in [\Omega, \pi]$. We choose the limits of integration as such, in order to take into account larger structures that are shed closer to the wedge and will contribute the most to the sound field according to the theory presented by Ffowcks Williams and Hall [24]. At large distances from the edge the source term becomes weaker and hence the contribution to the

sound field from sources located at $(r_0, \theta_0) = (X, \Omega)$ is negligible with respect to those located at $(r_0, \theta_0) = (\xi, \Omega)$. The exponential can be written as a sum of Bessel functions using the Jacobi-Anger expansion formula [30] :

$$e^{iz \cos(\theta_0)} = J_0(z) + 2 \sum_{j \geq 1} i^j J_j(z) \cos(j\theta_0) \quad (28)$$

where $z = \frac{\omega r_0}{U}$. Since $k_0 r_0 \ll 1$, the source distance with respect to the hydrodynamic wave-number $\frac{\omega r_0}{U}$ is of order $O(1)$ when the Mach number is $M \approx 0.1 - 0.2$. As a result, the Jacobi-Anger expansion formula can be truncated at different values of n depending on the argument $\frac{\omega r_0}{U}$. A more thorough comparison is shown in Fig. 4. The relative error of truncation is calculated for different values of $n = j_{max}$ and argument z . The angle θ is set to 0 in order to calculate the error for the strictest case. It can be seen that for low Mach numbers, if $n > 50$ the maximum relative error is less than 5%. Thus, the response of a convected turbulent fluctuation close to the edge of the wedge is given by

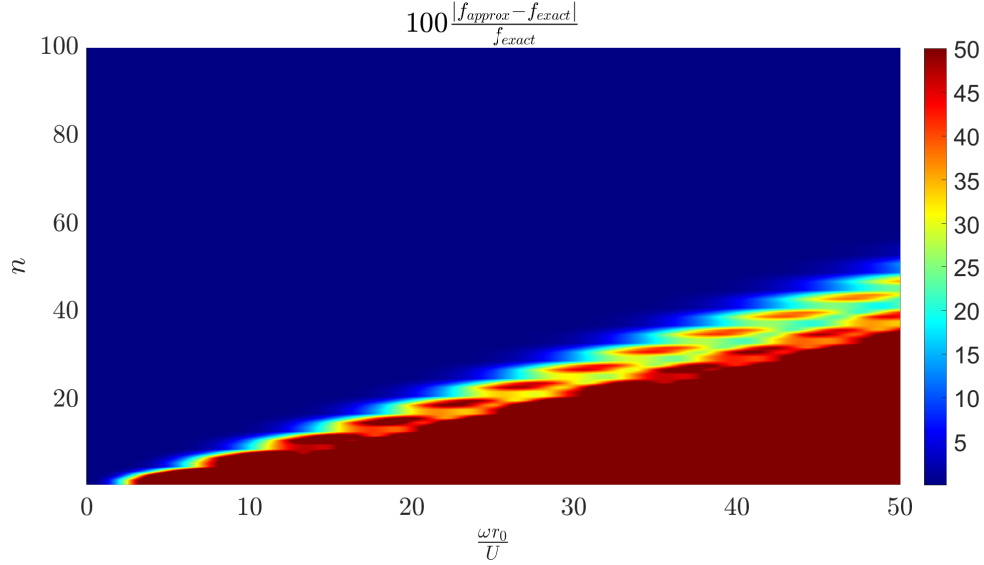


Fig. 4 Maximum relative error of the truncation of the infinite series in Eq. (28). The function f_{exact} corresponds to left hand side of Eq. (28), while f_{approx} to the right hand side for different values of n . The errors are depicted for the strictest case when $\theta_0 = 0$.

$$R_{out} = -\frac{e^{i(k_0|\vec{r}|-\pi/(2\gamma))} (k_0 \sin \psi/2)^{1/\gamma}}{\gamma^2 \pi |\vec{r}| \Gamma(1/\gamma + 1)} \cos\left(\frac{\theta - \pi}{\gamma}\right) \times \quad (29)$$

$$\times \int_{\xi}^X \int_{\theta_{0,1}}^{\theta_{0,2}} r_0^{1/\gamma} \sin\left(\frac{\pi + (\gamma - 1)\theta_0}{\gamma}\right) \left(J_0\left(\frac{\omega r_0}{U}\right) + 2 \sum_{j \geq 1}^n i^j J_j\left(\frac{\omega r_0}{U}\right) \cos(j\theta_0) \right) dr_0 d\theta_0$$

For the current analysis, we take $n = 150$. By exploiting the symmetry of the problem (see Fig. 3) we perform the integration over $\theta_0 \in [\Omega, \pi]$. Since the infinite series of Eq.(28) is replaced by a finite sum, it is permitted to interchange the integral and summation signs. Hence it follows:

$$R_{out} = M^{1/\gamma} \left(\frac{U}{\omega}\right) \frac{2 \cos\left(\frac{\theta - \pi}{\gamma}\right) e^{i(k_0|\vec{r}|-\pi/(2\gamma))} (\sin \psi/2)^{1/\gamma}}{\gamma^2 \pi |\vec{r}| \Gamma(1/\gamma + 1)} \times \quad (30)$$

$$\times \left(\frac{2(\pi - \Omega)(\sin(\Omega) - 1)}{\pi - 2\Omega} I_0\left(\frac{\omega X}{U}\right) - \sum_{j \geq 1}^n A_j I_j\left(\frac{\omega X}{U}\right) \right)$$

where

$$A_j = -\frac{2i^j (\pi - \Omega) ((\pi - 2\Omega) (\cos(\pi j) - \sin(\Omega) \cos(j\Omega)) + 2j (\pi - \Omega) \cos(\Omega) \sin(j\Omega))}{(\pi (2j - 1) - 2(j - 1)\Omega) (-2(n + 1)\Omega + 2\pi j + \pi)} \quad (31)$$

The integrals of Eq. (30) can be written in the following form.

$$I_0\left(\frac{\omega X}{U}\right) = \int_{\frac{\omega \varepsilon}{U}}^{\frac{\omega X}{U}} \left(\frac{\omega r_0}{U}\right)^{1/\gamma} J_0\left(\frac{\omega r_0}{U}\right) d\left(\frac{\omega r_0}{U}\right) \quad (32)$$

$$I_j\left(\frac{\omega X}{U}\right) = \int_{\frac{\omega \varepsilon}{U}}^{\frac{\omega X}{U}} \left(\frac{\omega r_0}{U}\right)^{1/\gamma} J_j\left(\frac{\omega r_0}{U}\right) d\left(\frac{\omega r_0}{U}\right)$$

It can be seen that larger convected eddies contribute more to the lower frequency regime, while those that lie in the inner region become more and more important noise sources with respect to the latter at higher frequencies and larger wedge angles. This becomes more apparent by considering the fraction of the response functions.

$$\frac{R_{in}}{R_{out}} = \left| \frac{\left(\frac{2(\pi - \Omega)(\sin(\Omega) - 1)}{\pi - 2\Omega}\right) \int_{\frac{\omega \varepsilon}{U}}^{\frac{\omega X}{U}} e^{i\alpha} \alpha^{1/\gamma} d\alpha}{\left(\frac{2(\pi - \Omega)(\sin(\Omega) - 1)}{\pi - 2\Omega}\right) I_0\left(\frac{\omega X}{U}\right) - \sum_{j \geq 1}^n A_j I_j\left(\frac{\omega X}{U}\right)} \right| \quad (33)$$

Figure 5 shows a comparison of the response functions presented in the previous subsections. It is noted that some local maxima are observed at higher non-dimensional frequencies and wedge angles. These correspond to local minima of R_{out} .

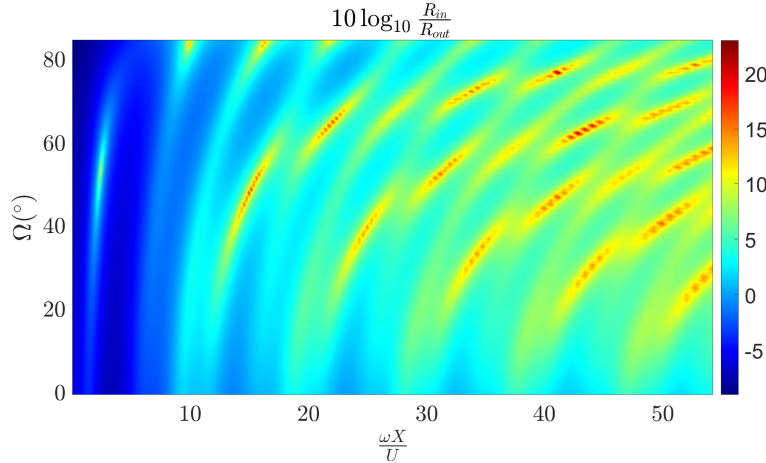


Fig. 5 Comparison of the response functions that correspond to the inner region (Eq. (30)) and the outer region close to the wedge (Eq. (27)).

V. Turbulence modelling

Equations (27), (30) describe the scattering of a sound source (smaller and larger eddies) very close to the edge of the wedge. The radiation properties of the source (directivity, spectra, maximum amplitude etc.) are included in the turbulent spectra, which can be obtained by experiments numerical simulations or empirical/ analytical models. In the present case and for purposes of illustration, the vorticity spectrum tensor ϕ_{ij} is described as shown by Howe in [20].

$$\phi_{ij} = \frac{E(k)}{4\pi k^2} (k^2 \delta_{ij} - k_i k_j) \quad (34)$$

where

$$E(k) = \frac{55\Gamma(5/6) \langle u^2 \rangle l^5 k^4}{27\sqrt{\pi}\Gamma(1/3) (1 + (kl)^2)^{17/6}}$$

is the von Karman turbulence spectrum, l the turbulence correlation scale and $k = \sqrt{\frac{\omega^2}{U^2} + k_2^2}$. Hence the turbulent spectra are given by

$$\Phi^{(2)} = \frac{55\Gamma(5/6)\langle u^2 \rangle \omega^2 U^2 l_{in}^5}{27\sqrt{\pi}\Gamma(1/3)} \int_0^\infty \frac{\left(\frac{\omega^2}{U^2} + k_2^2\right)^2}{\left(1 + l_{in}^2 \left(\frac{\omega^2}{U^2} + k_2^2\right)^2\right)^{17/6}} dk_2 \quad (35)$$

$$\Xi^{(2)} = \frac{55\Gamma(5/6)\langle u^2 \rangle \omega^2 U^2 (l_{out})^5}{27\sqrt{\pi}\Gamma(1/3)} \int_0^\infty e^{ik_2 l_{out}} \frac{\left(\frac{\omega^2}{U^2} + k_2^2\right)^2}{\left(1 + (l_{out})^2 \left(\frac{\omega^2}{U^2} + k_2^2\right)^2\right)^{17/6}} dk_2$$

where $\frac{1}{2}\langle u^2 \rangle \approx \frac{1}{2}U^2$ the mean turbulent kinetic energy. The two length scales of Equation (35) correspond to the correlation length scales inside the two different regions of Fig. 2. The power spectra of the turbulent kinetic energy of each region are shown in Figure 6. As expected, larger scales dominate at lower frequencies, while at higher frequencies the turbulent kinetic spectrum is greater for smaller eddies.

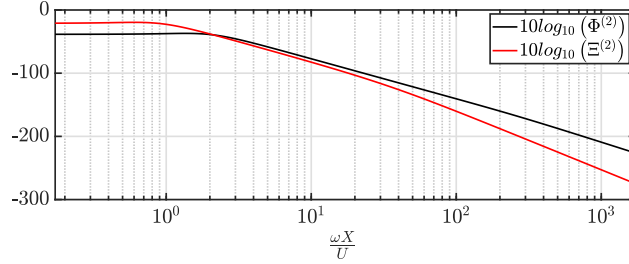


Fig. 6 Vorticity correlation spectra for the inner ($\Phi^{(2)}$) and outer ($\Xi^{(2)}$) region. The correlation length is considered to be $l_{out} = d/5$ for the outer region and $l_{in} = l_{out}/5$ for the inner region.

The far field power spectral density

$$PSD_{in/out} = 10 \log_{10} \frac{\langle PP^* \rangle_{in/out}}{P_{ref}^2}$$

is depicted for each region and different wedge angles in Figure 7. The results are shown for an airfoil with chord $d = 0.15m$ and span $L = 1m$. Assuming that the results do not vary across the span, we set $l_{y_3}(\omega) = L$. For purposes of illustration, the wake extent is taken equal to one chord of the airfoil $X = d$. For the inner region we choose $\epsilon = 10^{-6}m$ and $\xi = d/5$. The far field power spectral density is estimated for a mean velocity of $U = 30m/s$ and an observer in the far field at $r = 10d$ and $\theta = \gamma\pi/2$, so that the radiation peak can be recorded for every wedge angle. The results are shown for wedge angles starting from $\Omega = 0$ (half plane) up to $\Omega = 45^\circ$ (right angled wedge). The influence of each turbulent region can be seen clearly on the third plot of Fig.7. For low frequencies the larger eddies seem to be the dominant sound source, while the smaller inner region contributes more to the far field acoustic power spectral density at higher frequencies. The increase of the wedge angle leads to a reduction of the generated noise, which lies in agreement with the results presented in the literature [6], [7]. However, it should be noted that the effect of the wedge angle is not taken into account for the modelling of the flow field. In some cases, the wedge angle favours the separation of the flow at the trailing edge which may lead to shedding of periodic structures that result in tonal noise, which cannot be predicted by the current turbulent model [26]. From Eqs (27), (30),(35) it can be observed that the acoustic power spectral density scales to:

$$\langle PP^* \rangle \sim U^2 \langle u^2 \rangle U^{2/\gamma} \approx U^{2/\gamma+4} \quad (36)$$

When the wedge problem reduces to the one of the half plane ($\gamma = 2$), the present model scales with the same law as the one proposed by Ffowcs Williams and Hall (1969). Moreover, Eq. (36) is exactly the same as the one derived

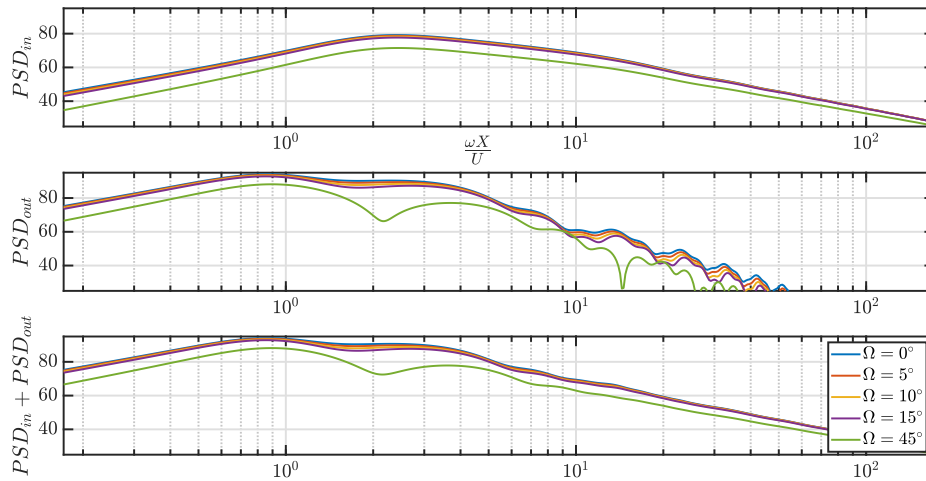


Fig. 7 Far field power spectra density for the inner and outer region, obtained by Eq.(18). The results are shown for a mean velocity is $U = 30m/s$, an observer in the far field at $r = 10d$ and $\theta = \gamma\pi/2$ and different wedge angles.

by Crighton and Leppington [7]. Their work, however, was restricted in physical analysis and derivation of scaling laws, when quadruple sources are scattered by acoustically compact, hard and soft wedge like objects, using Lighthill's acoustic analogy. The difference with the present study is that our analysis is extended in deriving an analytical solution for estimation of the acoustic far field power spectral density by using a formulation similar to Amiet's model, while employing Howe's aeroacoustic analogy.

VI. Conclusions

We have studied a simple analytical model for the estimation of the far-field acoustic power spectral density associated with a turbulent flow impinging on a wedge with an arbitrary angle. Overall, the proposed model was based on the framework of Amiet's work [9]. However, we used Howe's theory of vortex sound to model the source, and took into account a turbulent vorticity spectrum [20] to the proximity of the edge of an arbitrary wedge. The asymptotic expressions of the Green function for the acoustic scattering around a rigid wedge was employed, which allows a better description of the scattering at low frequencies as the solution of the Laplace's equation shown in [7], since the dependence on the main parameters is explicit and there are no arbitrary amplitude factors. The turbulent region around the edge was split into: i) smaller eddies that lie close to the edge, with a turbulent length scale comparable to their distance from the edge and ii) larger eddies where the convection effect is considered. The amplitude of the far-field acoustic power spectral density is found to increase for sharper wedges and lower frequencies. This result is in agreement with other studies in the literature. It has been shown experimentally [26] and theoretically [31] that the larger the angle of a bevelled trailing edge the less far field noise is generated. The advantage of the presented model is that the problem of aerodynamic sound generation on a rigid wedge allows a broader description of the edge noise and encompasses the case of the half-plane. The wedge angle can be used to approximate the thickness of leading and trailing edges, while it is possible to model other types of air-frame noise, as long as the turbulent spectrum is known. For instance, the side-edge-flap noise is studied by considering a right angled wedge with $\Omega = \pi/4$ [27]. However, our analysis does not consider the influence of the wedge angle on the flow field. This work can be extended to higher frequencies by taking into account the exact Green's function (Eq. (20)) and using more realistic turbulent spectra deduced from experiments or numerical simulations. Furthermore, it is observed that there is also another mechanism of sound generation that depends on non-linear terms ($\langle \Omega_{ij}^2 \rangle$), as shown in (Eq. (12)) and should be examined in more detail.

Acknowledgements

This work was supported by the DGAC (Direction Générale de l'Aviation Civile), by the PNRR (Plan National de Relance et de Résilience Français) and by NextGeneration EU via the project MAMBO (Méthodes Avancées pour la Modélisation du Bruit moteur et aviOn).

References

- [1] Boudet, J., Grosjean, N., and Jacob, M. C., "Wake-airfoil interaction as broadband noise source: a large-eddy simulation study," *International Journal of Aeroacoustics*, Vol. 4, No. 1-2, 2005, pp. 93–115.
- [2] Jacob, M. C., Boudet, J., Casalino, D., and Michard, M., "A rod-airfoil experiment as a benchmark for broadband noise modeling," *Theoretical and Computational Fluid Dynamics*, Vol. 19, 2005, pp. 171–196.
- [3] Lee, S., Ayton, L., Bertagnolio, F., Moreau, S., Chong, T. P., and Joseph, P., "Turbulent boundary layer trailing-edge noise: Theory, computation, experiment, and application," *Progress in Aerospace Sciences*, Vol. 126, 2021, p. 100737.
- [4] Lighthill, M. J., "On sound generated aerodynamically I. General theory," *Proceedings of the Royal Society of London. Series A. Mathematical and Physical Sciences*, Vol. 211, No. 1107, 1952, pp. 564–587.
- [5] Curle, N., "The influence of solid boundaries upon aerodynamic sound," *Proceedings of the Royal Society of London. Series A. Mathematical and Physical Sciences*, Vol. 231, No. 1187, 1955, pp. 505–514.
- [6] Williams, J. F., and Hawkings, D. L., "Sound generation by turbulence and surfaces in arbitrary motion," *Philosophical Transactions for the Royal Society of London. Series A, Mathematical and Physical Sciences*, 1969, pp. 321–342.
- [7] Crighton, D., and Leppington, F., "On the scattering of aerodynamic noise," *Journal of Fluid Mechanics*, Vol. 46, No. 3, 1971, pp. 577–597.
- [8] Chase, D. M., "Sound radiated by turbulent flow off a rigid half-plane as obtained from a wavevector spectrum of hydrodynamic pressure," *The Journal of the Acoustical Society of America*, Vol. 52, No. 3B, 1972, pp. 1011–1023.
- [9] Amiet, R. K., "Acoustic radiation from an airfoil in a turbulent stream," *Journal of Sound and vibration*, Vol. 41, No. 4, 1975, pp. 407–420.
- [10] Amiet, R. K., "Noise due to turbulent flow past a trailing edge," *Journal of sound and vibration*, Vol. 47, No. 3, 1976, pp. 387–393.
- [11] Roger, M., and Moreau, S., "Back-scattering correction and further extensions of Amiet's trailing-edge noise model. Part I: theory," *Journal of Sound and vibration*, Vol. 286, No. 3, 2005, pp. 477–506.
- [12] Moreau, S., and Roger, M., "Back-scattering correction and further extensions of Amiet's trailing-edge noise model. Part II: Application," *Journal of Sound and vibration*, Vol. 323, No. 1-2, 2009, pp. 397–425.
- [13] Zhong, S., Zhang, X., Peng, B., and Huang, X., "An analytical correction to Amiet's solution of airfoil leading-edge noise in non-uniform mean flows," *Journal of Fluid Mechanics*, Vol. 882, 2020.
- [14] Trafny, N., Serre, G., Cotté, B., and Mercier, J.-F., "A stochastic volume approach based on tailored Green's functions for airfoil noise prediction at low Mach number," *Journal of Sound and Vibration*, Vol. 551, 2023, p. 117603.
- [15] Howe, M. S., "Edge-source acoustic Green's function for an airfoil of arbitrary chord, with application to trailing-edge noise," *Quarterly Journal of Mechanics and Applied Mathematics*, Vol. 54, No. 1, 2001, pp. 139–155.
- [16] Howe, M., "Contributions to the theory of aerodynamic sound, with application to excess jet noise and the theory of the flute," *Journal of Fluid Mechanics*, Vol. 71, No. 4, 1975, pp. 625–673.
- [17] Howe, M. S., *Aerodynamic sound in unbounded flows*, Cambridge Monographs on Mechanics, Cambridge University Press, 1998, p. 101–156. <https://doi.org/10.1017/CBO9780511662898.003>.
- [18] Howe, M. S., "A review of the theory of trailing edge noise," *Journal of sound and vibration*, Vol. 61, No. 3, 1978, pp. 437–465.
- [19] Gershfeld, J., "Leading edge noise from thick foils in turbulent flows," *The Journal of the Acoustical Society of America*, Vol. 116, No. 3, 2004, pp. 1416–1426.
- [20] Howe, M. S., *Sound generation in a fluid with rigid boundaries*, Cambridge Monographs on Mechanics, Cambridge University Press, 1998, p. 157–252. <https://doi.org/10.1017/CBO9780511662898.004>.

- [21] Margnat, F., and Gloerfelt, X., “On compressibility assumptions in aeroacoustic integrals: A numerical study with subsonic mixing layers,” *The Journal of the Acoustical Society of America*, Vol. 135, No. 6, 2014, pp. 3252–3263.
- [22] Howe, M. S., *Vortex Sound*, Cambridge Texts in Applied Mathematics, Cambridge University Press, 2002, p. 114–135. <https://doi.org/10.1017/CBO9780511755491.006>.
- [23] Goldstein, M. E., “Unsteady vortical and entropic distortions of potential flows round arbitrary obstacles,” *Journal of Fluid Mechanics*, Vol. 89, No. 3, 1978, p. 433–468. <https://doi.org/10.1017/S0022112078002682>.
- [24] Williams, J. E. F., and Hall, L. H., “Aerodynamic sound generation by turbulent flow in the vicinity of a scattering half plane,” *Journal of Fluid Mechanics*, Vol. 40, No. 4, 1970, p. 657–670. <https://doi.org/10.1017/S0022112070000368>.
- [25] Howe, M. S., “Trailing edge noise at low Mach numbers,” *Journal of Sound and Vibration*, Vol. 225, No. 2, 1999, pp. 211–238.
- [26] Celik, A., Bowen, J. L., and Azarpeyvand, M., “Effect of trailing-edge bevel on the aeroacoustics of a flat-plate,” *Physics of Fluids*, Vol. 32, No. 10, 2020, p. 105116.
- [27] Roger, M., Moreau, S., and Kucukcoskun, K., “On sound scattering by rigid edges and wedges in a flow, with applications to high-lift device aeroacoustics,” *Journal of Sound and Vibration*, Vol. 362, 2016, pp. 252–275.
- [28] Abramowitz, M., and Stegun, I. A., “Handbook of mathematical functions with formulas, graphs, and mathematical tables,” *Appl*, 1972.
- [29] Chang, C.-C., and Chen, T.-L., “Acoustic emission by a vortex ring passing near a sharp wedge,” *Proceedings of the Royal Society of London. Series A: Mathematical and Physical Sciences*, Vol. 445, No. 1923, 1994, pp. 141–155.
- [30] Cuyt, A. A., Petersen, V., Verdonk, B., Waadeland, H., and Jones, W. B., *Handbook of continued fractions for special functions*, Springer Science & Business Media, 2008.
- [31] Howe, M., “The influence of surface rounding on trailing edge noise,” *Journal of sound and vibration*, Vol. 126, No. 3, 1988, pp. 503–523.

A. Derivation steps of far-field acoustic power spectral density

In this appendix we show the steps of derivation Eq. 15. The procedure is the same as the one described in Amiet’s paper [10]. However, due to different assumptions regarding the source term, we show the analysis in more detail. From Equation 14 we have

$$\langle PP^* \rangle (\vec{x}, \omega) = -\rho^2 l_{y_3} (\omega) \int_{-\infty}^{\infty} \left[\int_0^{\infty} \phi_{ij}^m (\omega/U, k_2, 0) e^{i(k_2(y_2-y'_2))} dk_2 \right] \frac{\partial G}{\partial y_m} \frac{\partial G^*}{\partial y'_m} e^{i(\frac{\omega}{U}(y_1-y'_1))} dy_1 dy_2 dy'_1 dy'_2 \quad (\text{A.1})$$

For the inner region We set

$$\Phi^m = \int_0^{\infty} \phi_{ij}^m dk_2$$

where $m = 1, 2$ denotes the component in the stream-wise or transverse axis (y_1, y_2) . Furthermore, based on the assumptions of sub-section IV.A:

$$\frac{\omega}{U} (y_1 - y'_1) = \frac{\omega l_{in}}{U} \gg k_2 (y_2 - y'_2)$$

we may express Eq. (A.1) as

$$\langle PP^* \rangle_{in} (\vec{x}, \omega) = -\rho^2 l_{y_3} (\omega) \iiint_{-\infty}^{\infty} \Phi^m \frac{\partial G}{\partial y_m} \frac{\partial G^*}{\partial y'_m} e^{i\frac{\omega l_{in}}{U}} dy_1 dy_2 dy'_1 dy'_2 \quad (\text{A.2})$$

Furthermore, we define the response function, for the inner region, of an eddy interacting with the edge as:

$$R_{in,m} = \iint_{-\infty}^{\infty} \frac{\partial G}{\partial y_m} e^{i\frac{\omega l_{in}}{U}} dy_1 dy_2 \quad (\text{A.3})$$

similarly for the source at (y'_1, y'_2, y_3)

$$R_{in_m}^* = \iint_{-\infty}^{\infty} \frac{\partial G^*}{\partial y'_m} e^{i \frac{\omega l_{in}}{U}} dy'_1 dy'_2 \quad (\text{A.4})$$

where R_{in}^* , the complex conjugate of R_{in} , hence

$$R_{in}^* R_{in} = |R_{in}|^2$$

As a result the far-field acoustic power spectra density for the inner region becomes:

$$\langle PP^* \rangle_{in}(\vec{x}, \omega) = -\rho^2 \Phi^m |R_{in_m}|^2 l_{y_3}(\omega) \quad (\text{A.5})$$

The same procedure is used for the outer region (Eq. (17)).